Since January 2020 Elsevier has created a COVID-19 resource centre with free information in English and Mandarin on the novel coronavirus COVID-19. The COVID-19 resource centre is hosted on Elsevier Connect, the company's public news and information website.

Bone 44 (2009) 345–356

Contents lists available at ScienceDirect

Bone

journal homepage: www.elsevier.com/locate/bone

A novel semisynthesized small molecule icaritin reduces incidence of steroid-associated osteonecrosis with inhibition of both thrombosis and lipid-deposition in a dose-dependent manner

Ge Zhang [a], Ling Qin [a,*], Hui Sheng [a], Xin-Luan Wang [a,b], Yi-Xiang Wang [d], David Ka-Wai Yeung [d], James F. Griffith [d], Xin-Sheng Yao [b], Xin-Hui Xie [a], Zi-Rong Li [c], Kwong-Man Lee [e], Kwok-Sui Leung [a]

[a] Musculoskeletal Research Laboratory, Department of Orthopaedics & Traumatology, the Chinese University of Hong Kong, Shatin, N.T. Hong Kong SAR
[b] School of Chinese Materia Medica, Shenyang Pharmaceutical University, Shenyang, China
[c] Center for Osteonecrosis and Joint Preserving and Reconstruction, Department of Orthopaedic Surgery, Sino-Japan Friendship Hospital, Beijing, China
[d] Department of Diagnostic Radiology and Organ Imaging, the Chinese University of Hong Kong, Hong Kong SAR
[e] Lee Hysan Clinical Medicine, the Chinese University of Hong Kong, Hong Kong SAR

ARTICLE INFO

Article history:
Received 14 May 2008
Revised 7 September 2008
Accepted 3 October 2008
Available online 22 October 2008
Edited by: H. Genant

Keywords:
Steroid-associated osteonecrosis
Icaritin
Intravascular thrombosis
Extravascular lipid-deposition
MicroCT-based angiography
Dynamic MRI-based perfusion function

ABSTRACT

Background: Intravascular-thrombosis and extravascular-lipid-deposition are the two key pathogenic events considered to interrupt intraosseous blood supply during steroid-associated osteonecrosis (ON) development. However, there are no reported candidate agents capable of simultaneously targeting these two key pathogenic events. The authors' published experimental studies have shown that Epimedium-derived flavonoids possess an anti-ON effect. Further, the authors have recently identified a small molecule Icaritin as an intestinal metabolite of Epimedium-derived flavonoids.

Objective: The present study was to evaluate the prevention effect of the available semisynthesized small molecule Icaritin on steroid-associated ON development in a rabbit model.

Methods: After receiving an established inductive protocol for inducing steroid-associated ON, eighty-four male 28-week-old New-Zealand white rabbits were divided into the following three daily oral administration groups, including low dose Icaritin group (L-ICT; $n=28$; 5 $mg{\cdot}kg^{-1}{\cdot}day^{-1}$), high dose Icaritin group (H-ICT; $n=28$; 10 $mg{\cdot}kg^{-1}{\cdot}day^{-1}$), and control vehicle group (CON; $n=28$). Before and after induction, dynamic contrast-enhanced MRI was performed on proximal femur for intra-osseous perfusion function index. Meanwhile, blood samples were examined for coagulation, fibrinolysis, lipid-transportation, endothelium injury, oxidative stress, and hepatocyte injury index, while marrow samples were quantified for adipogenic potential index of mesenchymal stem cell by in vitro culture and proliferator-activated receptor-gamma (PPARgamma) protein expression by western blot. At baseline, week 1 and 2 post-induction, 4, 8 and 16 rabbits in each group were sacrificed, respectively. After sacrifice, femora were dissected for micro-CT-based micro-angiography, followed by histological examination of ON lesion, intravascular thrombosis, extravascular fat-cell and vascular endothelial growth factor (VEGF) localized expression.

Results: The ON incidence in the L-ICT and H-ICT groups was both significantly lower than that in the CON group ($p<0.05$ for both). The ON incidence in the H-ICT group was significantly lower than that in the L-ICT group ($p<0.05$). A significant decrease in the vascularization index and a significant increase in the permeability index seen in the CON group was attenuated in the L-ICT group and almost prevented in the H-ICT group at week 1 post-induction. Reduced perfusion to vessel-like structural units was more rarely found in the H-ICT group than in the L-ICT group. Regarding intravascular thrombosis, a significant increase in the thrombotic vessel count, endothelium injury index, coagulation index, and a significant decrease in both the fibrinolysis and oxidative stress index in the CON group were attenuated in the L-ICT group and prevented in the H-ICT group. For extravascular lipid-deposition, a significant increase in the fat cell area fraction, adipogenic potential index, PPARgamma expression and lipid-transportation index in the CON group was attenuated in the L-ICT group and prevented in the H-ICT group. Increased immunoreactivity of VEGF in the CON group was attenuated in the L-ICT group and prevented in the H-ICT group. Regarding safety, the hepatocyte injury index did not show significant change from baseline in any group.

Conclusion: Icaritin, a novel semisynthesized small molecule with osteoprotective potential, exerts dose-dependent effect on reducing incidence of steroid-associated ON with inhibition of both intravascular thrombosis and extravascular lipid-deposition. Suppression of the up-regulated PPARgamma expression for

* Corresponding author. Fax: +852 26324618.
E-mail address: Lingqin@cuhk.edu.hk (L. Qin).

8756-3282/$ – see front matter
doi:10.1016/j.bone.2008.10.035

extravascular adipogenesis of mesenchymal stem cells and protection from activated oxidative stress for intravascular endothelium injury were found to be involved in the underlying mechanisms.

Introduction

Pulsed steroids are frequently prescribed as life-saving agents for serious infectious diseases such as Severe Acute Respiratory Syndrome (SARS) and Acquired Immune Deficiency Syndrome (AIDS), or disease modifying drug for chronic autoimmune disease such as systemic lupus erythematosus (SLE) and rheumatoid arthritis (RA). Steroid-associated osteonecrosis (ON) is a serious side effect of high dose steroid treatment. As patients with steroid-associated ON have generally poor surgical prognosis [1,2], it is highly desirable to develop pharmacological agents which may prevent its occurrence [3].

A consensus etiopathogenesis of steroid-associated ON has been recently unified on both intravascular thrombosis induced occlusion and extravascular lipid-deposition induced pressure, leading to impairment of intra-osseous blood supply [1,3,4]. An imbalance between coagulation and fibrinolysis resulting from endothelium injury induced by activated oxidative stress, which predisposes to both hypercoagulation and hypofibrinolysis, has consistently presented itself in the intravascular events [5,6]; while predominant lipid transportation to peripheral tissue and elevated adipogenesis via up-regulated proliferator-activated receptor-gamma (PPARgamma) expression is involved in the extravascular events [7,8]. Although it has been experimentally confirmed that a combined administration of an anticoagulant with a lipid-lowering agent may help prevent steroid-associated ON [9], the ideal strategy would be to simultaneously target both intravascular thrombosis and extravascular lipid deposition to prevent steroid-associated ON development [4].

Epidemiological data showed that there was a lower prevalence (5–6%) of ON in patients recovered from SARS who were frequently prescribed a crude flavonoid extract of “Bone Strengthening Chinese Herb” Epimedium during their rehabilitation in southern China [10], whereas there was a higher prevalence (32.7%) of ON in patients who were seldom prescribed a crude flavonoid extract of Epimedium in northern China [11]. Our previously published studies showed that, using our established rabbit model [12], Epimedium-derived flavonoids (EF, composed of seven flavonoid compounds with parent ring) (Fig. 1A) demonstrated beneficial effects in the prevention of steroid-associated ON with inhibition of both intravascular thrombosis and extravascular lipid-deposition in a dose-dependent manner [13,14]. Our more recent study on intestinal metabolism of EF has shown that a single molecule Icaritin (ICT) (Fig. 1B) may be involved in intestinal metabolism of those seven flavonoid compounds with parent ring in EF, which corresponds to the recent consensus that diversiform isoflavones with a parent ring may be intestinally metabolized to a single Equal for acting on pharmacological targets [15,16] and Icaritin may be involved in enzymatic hydrolysis of prenylated flavonols [17].

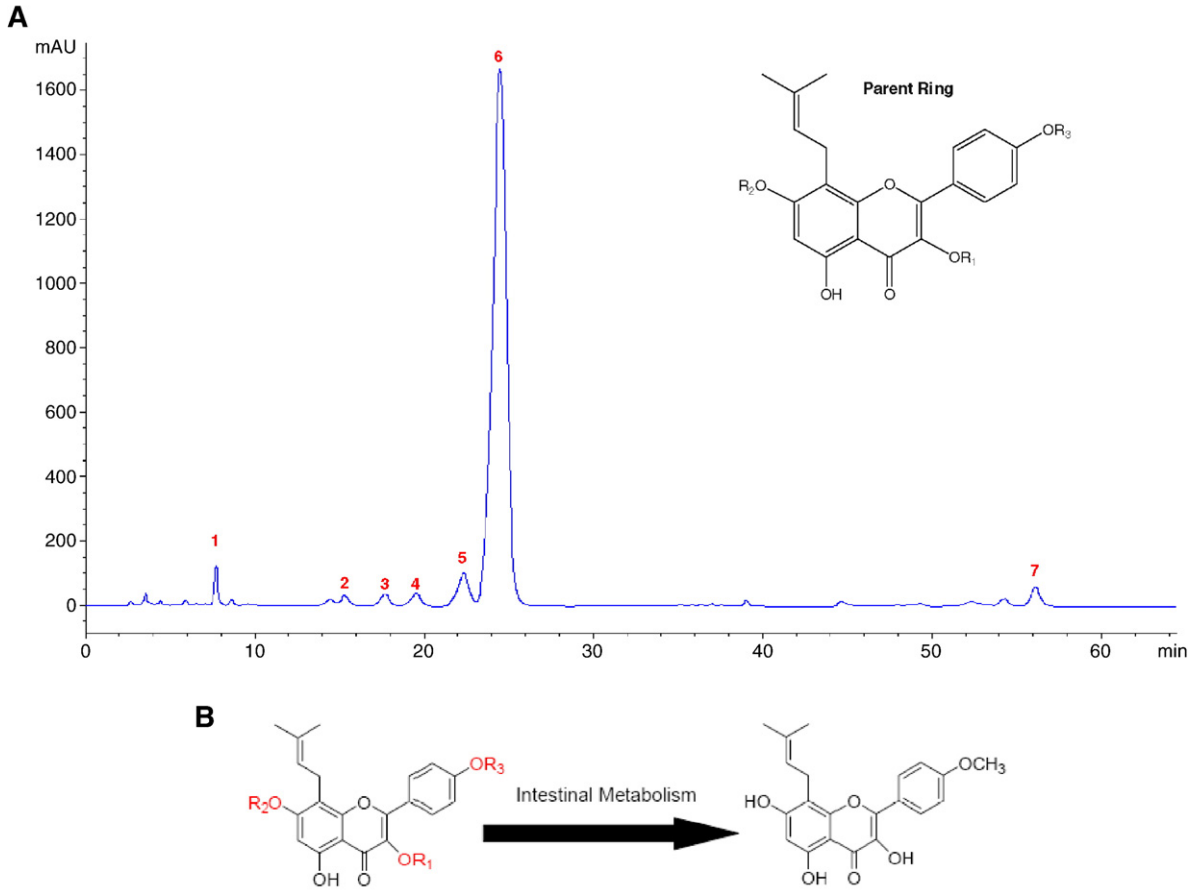

Fig. 1. Phytochemical and metabolic information on EF. (A) Seven major flavonoid molecules (1=epimedoside A, 2=hexandraside F, 3=epimedin A, 4=epimedin B, 5=epimedin C, 6=Icaritin and 7=baohuoside-I) identified in Epimedium-derived flavonoids. The parent ring is 8-prenylkaempferol. R1 and R2 are substituted by glucose, rhamnose, or xylose, and R3 is replaced by methyl. (B) Epimedium-derived flavonoids with parent ring are metabolized in the intestine to Icaritin.

As there were no available studies addressing the dose-dependent effect as well as the underlying mechanism of Icaritin in preventing steroid-associated ON development, the present study was accordingly designed to use our established rabbit model to examine the dose-dependent effect of Icaritin by evaluation on molecular, cytological, and haematological indices for intravascular thrombosis and extravascular lipid-deposition, dynamic contrast-enhanced MRI based perfusion function indices, micro-CT based angiography, histopathological indices for ON lesion, intravascular thrombosis and extravascular lipid-deposition, and local vascular endothelial growth factor (VEGF) expression.

Materials and methods

Animal, group and treatment

Eighty-four male 28-week-old New-Zealand white rabbits with body weight of 4–5 kg were housed at the Laboratary Animal Service Center of Prince of Wales Hospital, the affiliated hospital of the Chinese University of Hong Kong. The animals received a standard laboratory diet and water *ad libitum*. The experimental protocol was approved by the Animal Experiment Ethics Committee of the Chinese University of Hong Kong (Ref No.04/038/MIS). Based on our established protocol for inducing steroid-associated ON [12], all rabbits were intravenously injected with 10 μg. kg^{-1} of lipolysaccharide (LPS; *Escherichia coli* 0111:B4, Sigma-Aldrich, Inc. USA) on day 0 (week 0). 24 h later, three injections of 20 mg. kg^{-1} of methylprednisolone (MPS; Pharmacia & Upjohn, USA) were given intramuscularly at a time interval of 24 h. Thereafter, the rabbits were divided into the following three daily oral administration groups: low dose Icaritin group (L-ICT; n=28; 5 mg. kg^{-1}. day^{-1}), high dose Icaritin group (H-ICT; n=28; 10 mg. kg^{-1}. day^{-1}), and control vehicle group (CON; n=28).

Preparation for Icaritin

Based on our standardized procedure (acid hydrolysis and then purification), 30 g Epimedium-derived flavonoids were taken in 1 N HCl-40% ethanol solution (v/v) at 20 times concentration (v/w) and heated to reflux in a water bath at 70 °C for 10 h to hydrolyze sugars bonded to aglycone. The reaction was concentrated under pressure to remove the solvent. The residue was added to 300 ml ethanol, stirred 3 times and filtrated to remove precipitated salts. The filtrate was concentrated under pressure to obtain a crude product, which was purified by silica gel column chromatography, charged with silica 150 g gel. Chloroform and methanol were used as eluting solvents. Fractions were obtained by increasing the ratio of chloroform and methanol from 10:1 to 2:1, such that 4.2 g of Icaritin was produced. Icaritin was structurally identified by ESI-MS and NMR, and purity was confirmed at 98.6% by high performance liquid chromatography (HPLC).

Pre-euthanasia evaluation

At week 0 (immediately before LPS injection), 1 and 2 post-induction, blood sample was taken for examination on coagulation index (APTT, i.e. activated partial thromboplatin time) [12,13], fibrinolysis index (t-PA/PAI-I, i.e. ratio of tissue type plasminogen activator to plasminogen activator inhibitor) [12,13], lipid-transportation index (LDL/HDL, i.e. ratio of low density lipoprotein cholesterol to high density lipoprotein cholesterol) [12,13], endothelium injury index (TM, i.e. thrombomodulin) [39,40], oxidative stress index (GSH/LPO, i.e. ratio of glutathione to lipid peroxide) [6], and hepatocyte injury index (GPT, i.e. glutamate-pyruvate transaminase). Marrow samples from iliac crest were obtained for evaluation on adipogenic potential index of mesenchymal stem cell (adipocyte

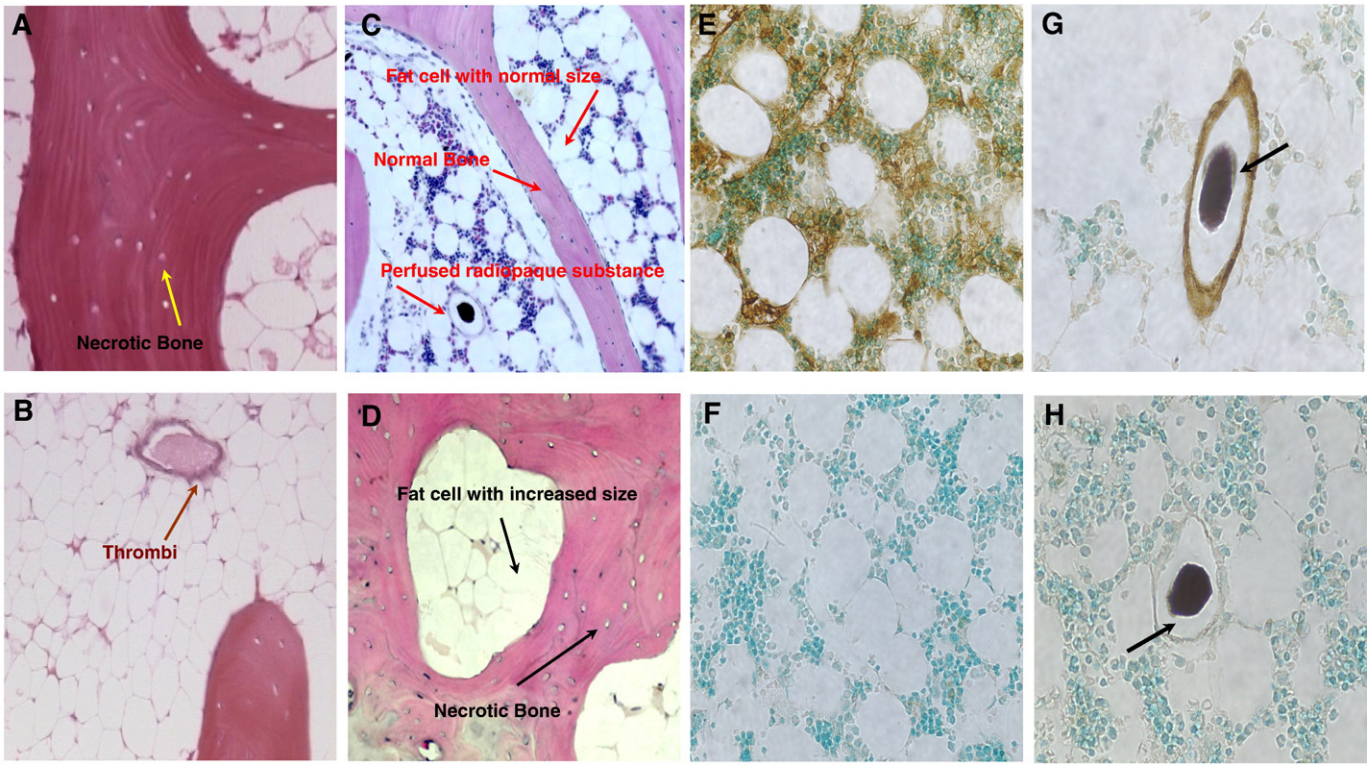

Fig. 2. Key characteristics during histopathological identification. (A) ON lesion was shown by trabecular bone containing many empty lacunae. (B) In ON^+ rabbits, thrombi were predominantly found in small marrow vessels in ON^+ rabbits, and marrow was mainly occupied by numerous fat cells with increased size in ON^+ rabbits (D) compared to normal rabbits (C). Strong immunoreactivity was found in both marrow cells (E) and endothelium (G) in the CON group at week 1 and 2 post-induction. Weak immunoreactivity was found in both marrow cells (F) and endothelium (H) in either the baseline or H-ICT group at week 1 and 2 post-induction. Baseline information not shown here. Arrow pointed particles in G and H were angiographic substance.

positvie colonies) and proliferator-activated receptor-gamma (PPAR-gamma) protein expression at baseline (immediately before LPS injection, i.e. week 0), week 1 and week 2 post-induction [41]. Dynamic-contrast-enhanced MRI was performed on proximal femur for intra-osseous perfusion function index (vascularization index—PEP, i.e. 'peak enhancement percentage'; permeability index—PSρ, i.e. 'permeability surface area product per unit volume of tissue') before sacrifice at baseline, week 1, and week 2 post-induction, using a bolus of dimeglumin gadopentetate (Magnevist; Schering, Berlin, Germany) [12,13,42].

Post-euthanasia evaluation

Four, eight and sixteen rabbits in each group were sacrificed with overdose sodium pentobarbitone at baseline, week 1 and 2 post-induction. Under general and deep anesthesia with sodium pentobarbital, the abdomen cavity was opened for perfusion with a confected radiopaque silicone rubber, using our previously established protocol [13]. Then, the bilateral proximal femora were dissected for micro-CT-based three-dimensional (3-D) angiography after specimen decalcification, including a histogram generated to display size (thickness) distribution of angiographic structural units and a color-coded scale mapped to the surface of the 3-D images to provide a visual representation of size distribution of angiographic structural units [12,13]. Histopathological examination was performed to identify local ON lesion by established criteria, i.e. diffuse presence of empty lacunae or pyknotic nuclei of osteocytes in the trabeculae accompanied by surrounding necrotic bone marrow [43]. Each rabbit that had at least one ON lesion in the areas was considered as ON^+, while that without ON lesion was considered as ON^-. ON incidence was defined as numbers of ON^+ rabbits divided by numbers of total rabbits in each group, and ON extent was defined as numbers of ON lesions per ON^+ rabbit [12,13]. Intravascular thrombosis index (thrombotic vessle counts), extravascular lipid-deposition index (fat cell area fraction) [41] and size distribution of extravascular leakage particles during angiography were also quantified histomorphometrically [14,44]. Local vascular endothelial growth factor (VEGF) expression was graded by a semi-quantitative estimation of immunoreactivity: negative (−), weak (+), moderate (++), strong (+++) [45]. The body weight of each rabbit before sacrifice was documented and survival condition throughout the experiment period in each group was recorded.

Statistics

Categorial data, i.e. ON incidence, was analyzed using Fisher's exact probability test. Numeric data in each group was expressed as Mean ± SD. Hisopathological data was examined using Analysis of Covariance (ANOVA), using LSD' s post hoc multiple comparisons.

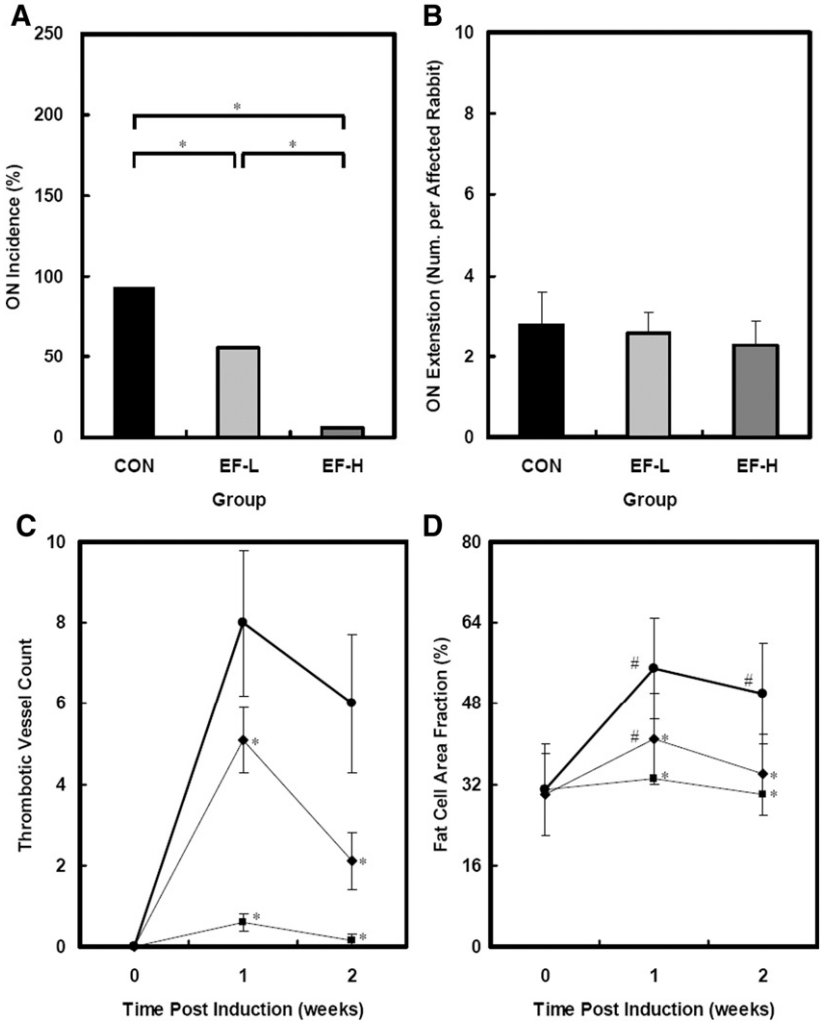

Fig. 3. Histopathological data analysis. (A) Incidence of ON in each group: CON (15/16, 93%), L-ICT (9/16, 56%) and H-ICT (1/16, 6%). (B) There was no significant difference in the ON extent among all the groups. (C) Thrombotic vessel count and (D) fat cell area fraction presented similar changes in over time, i.e. attenuated in the L-ICT group or prevented in the H-ICT group when compared to the CON group. Note: ● CON group, ♦ L-ICT group, ■ H-ICT group, and * $p<0.05$.

Longitudinal numeric data, i.e. dynamic perfusion MRI data, marrow molecular, cytological, and haematological data, were analyzed using 'ANOVA of Repeated Measures', using LSD's post hoc multiple comparisons. All statistical analysis were performed using SPSS 10.0. Statistical significance for compaison was set at $p<0.05$.

Results

Prevention efficacy and safety evaluation

GPT, as an index of hepatocyte injury, did not significantly change from baseline among all groups throughout the experimental period (data not shown here). No organ bleeding or death occurred in any group throughout the experimental period. ON lesion was not found until week 2 post-induction in any group. ON lesion was histopathologically characterized with trabecular bone containing empty lacunae with increased marrow fat cell size (Figs. 2A–D). The ON incidence was 93% (15/16) in the CON group, 56% (9/16) in the L-ICT group and 6% (1/16) in the H-ICT group. Fisher's exact probability test showed that the ON incidence in the L-ICT and H-ICT group was significantly lower than that in the CON group ($p<0.05$ for both). The ON incidence in the H-ICT group was significantly lower than that in the L-ICT group ($p<0.05$). There was no significant difference in the ON extent among the CON group (2.8±0.8), L-ICT group (2.6±0.5), and H-ICT group (2.3±0.6) (Figs. 3A, B).

Effect on intravascular/extravascular pathogenic events

Intravascular histopathology and contributing events

Histopathologically, thrombi were predominantly found in small marrow vessels in the CON group from week 1 post-induction (Figs. 2A, B). The thrombotic vessel count in the CON group peaked at week 1 post induciton, and maintained until week 2 post indcution. There was a signficant difference in the changing pattern of the thrombotic vessel counts between the CON group and two Icaritin groups. The increased thrombotic vessel count in the CON group was attenuated in the L-ICT group and prevented in the H-ICT group throughout the experimental period. The mangnitude of the thrombotic vessel count at week 1 post induction was similar to those at week 2 post indctuion, i.e. CON>L-ICT>H-ICT (Fig. 3D).

Both TM and APTT in the CON group increased significantly at week 1 post-induction ($p<0.00$ for both), then both declined toward baseline. There was a signficant difference in the changing pattern post-induction between the CON group and two Icaritin groups ($p<0.05$ for L-ICT vs CON and $p<0.01$ for H-ICT vs CON in both TM and APTT). In particular, the significant increase in both TM and APTT in the CON group were attenuated in the L-ICT group and almost prevented in the H-ICT group at week 1 post-induction (Figs. 4A, B).

Both tPA/PAI-I and GSH/LPO in the CON group significantly decreased at week 1 post-induction ($p<0.01$ for both), then returned toward baseline. There was a signficant difference in the changing pattern post-induction between the CON group and two Icaritin groups for both tPA/PAI-I and GSH/LPO ($p<0.05$ for L-ICT vs CON and $p<0.01$ for H-ICT vs CON in both tPA/PAI-I and GSH/). In particular, the significant decrease in both tPA/PAI-I and GSH/LPO in the CON group was attenuated in the L-ICT group and almost prevented in the H-ICT group at week 1 post-induction (Figs. 4C, D).

Extravascular histopathology and contributing events

Histopathologically, marrow was predominantly occupied by numerous fat cells in the CON group after induction (Figs. 2C, D).

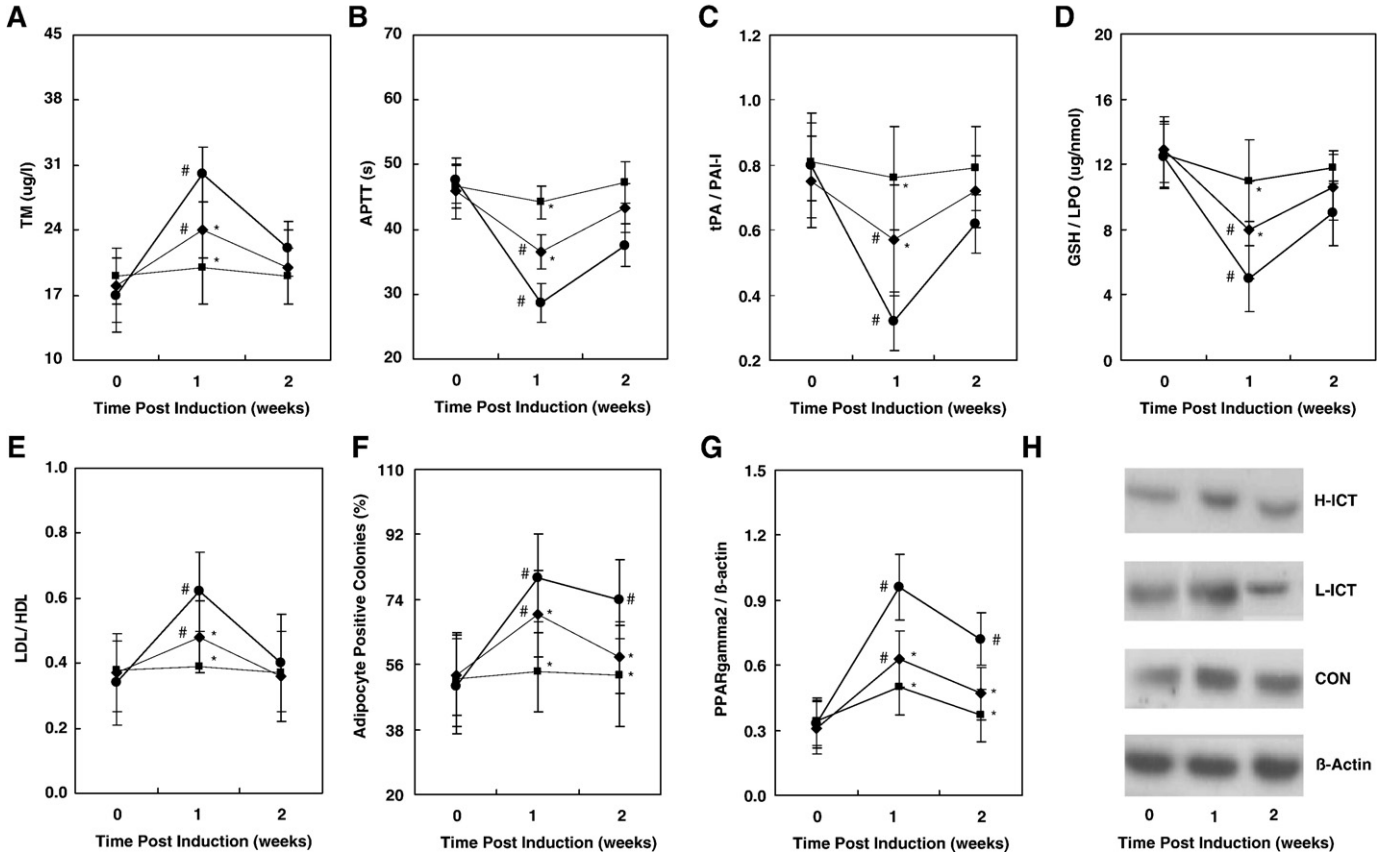

Fig. 4. Molecular-, hematological- and cytological data. Significantly decreased APTT (B), t-PA/PAI-I (C) and GSH/LPO (D) from baseline in the CON group were attenuated in the L-ICT group and prevented in the M-ICT and H-ICT group at week 1 post-induction, significantly increased TM (A), LDL/HDL (E), adipocyte positive colonies (F) and PPARgamma expression (G) from the baseline in the CON group were attenuated in the L-ICT group and prevented in the H-ICT group after induction. (H) A representative western blot image for PPARgamma protein expression corresponding to (G). Note: *p 0.05 for comparison with CON; # $p<0.05$ for comparison with baseline. ● CON group, ♦ L-ICT group, and ■ H-ICT group.

The fat cell area fraction in the CON group increased signficantly at week 1 post induciton, and this fraction maintained until week 2 post induction ($p<0.05$ for both). There was a signficant difference in the changing pattern post-induction between the CON group and two Icaritin groups. The significantly increased fat cell area fraction in the CON group was attenuated in the L-ICT group and prevented in the H-ICT group throughout the experimental period. The magnitude of fat cell area fraction at week 1 post indctuion was smilar to that at week 2 post indctuion, i.e. CON>L-ICT>H-ICT (Fig. 3C).

The adipocyte positive colonies, LDL/HDL and PPARgamma2 expression in the CON group increased significantly at week 1 post-induction ($p<0.01$ for all indices), thereafter moderately restored toward baseline for both the adipocyte positive colonies and PPARgamma2 expression, or returned to baseline for LDL/HDL. There was a significant difference in the changing pattern over time between the CON group and two Icaritin groups for the adipocyte positive colonies, LDL/HDL and PPARgamma2 expression ($p<0.05$ for L-ICT vs CON and $p<0.01$ for H-ICT vs CON in all indices). In particular, the significant increase in the adipocyte positive colonies, PPARgamma expression and LDL/HDL in the CON group were attenuated in the L-ICT group and almost prevented in the H-ICT group at week 1 post-induction (Figs. 4E–H).

Effect on intra-osseous vascular pathophysiology

Vascular perfusion function

The PEP in the CON group decreased significantly at week 1 post-induction ($p<0.01$), then significantly increased over baseline at week 2 post-induction ($p<0.01$). There was a significant difference in the changing pattern of the PEP over time between the CON group and two Icaritin groups ($p<0.01$ for L-ICT vs CON and $p<0.01$ for H-ICT vs CON). In particular, the significant decrease in the PEP in the CON group was attenuated in the L-ICT group and almost prevented in the H-ICT group at week 1 post-induction (Figs. 5A–C).

The PSρ in the CON group increased significantly at week 1 post-induction ($p<0.01$), further significantly increased at week 2 post-induction ($p<0.01$). There was a significant difference in the changing pattern of the PSρ over time between the CON group and two Icaritin groups ($p<0.05$ for CON group vs CON, and $p<0.01$ for H-ICT vs CON). In particular, the significant increase in the PSρ in the CON group was

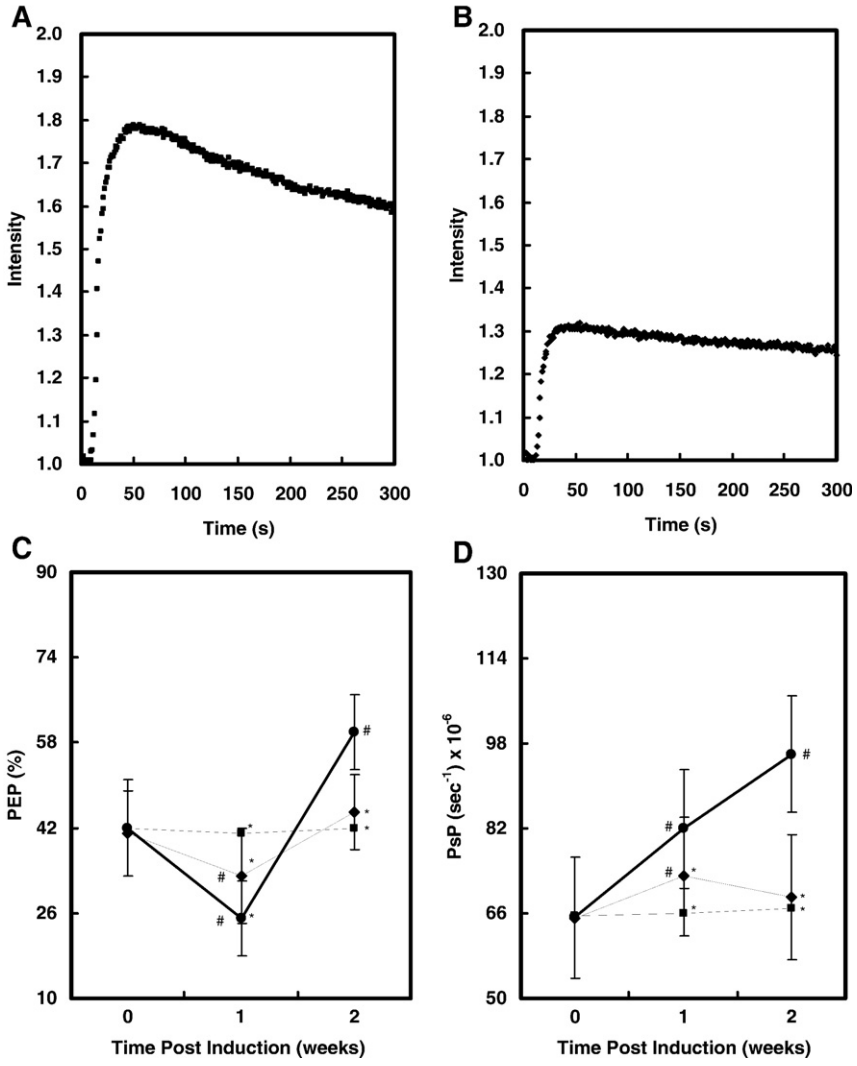

Fig. 5. Dynamic contrast-enhanced MRI data during longitudinal study, representative 3-D angiogram from micro-CT-based angiography and examination of perfused leakage particles for micro-CT-based angiography. Difference in representative dynamic contrast-enhanced MRI derived time-intensity curve at week 1 post-induction between the H-ICT group with high peak enhancement percentage (A) and the CON group with low peak enhancement percentage (B). (C) At week 1 post-induction, the significantly decreased PEP in the CON group was attenuated in the L-ICT group and prevented in the H-ICT group. (D) Throughout the experimental period, the significantly increased PSρ in the CON group were attenuated in the L-ICT group and almost prevented in the H-ICT group.

attenuated in the L-ICT group and almost prevented in the H-ICT group throughout the experimental period (Figs. 5A, B, D).

Intra-osseous vascular structure

Representative 3-D angiograms are shown in Figs. 6A–C, and representative histograms of the size of angiographic structural units are shown in Figs. 7A–H.

The angiograms in the CON group at week 1 post-induction showed dilated vessel-like structural units (>600 μm) surrounded by both numerous medium size widespread leakage-particle-like structural units (200–400 μm) and few vessel-like structural units (36–200 μm or 400–600 μm), when compared to those at baseline (Fig. 7A). The dilated vessel-like structural units (>600 μm) could be due to occlusion of downstream vessels (400–600 μm). The few vessel-like structural units (36–200 μm or 400–600 μm) could be explained by vessel occlusion. Relative to those in the CON group at week 1 post-induction, no typical dilated vessel-like structural units surrounded by numerous medium-sized widespread leakage-particle-like structural units (200–400 μm) (also confirmed histologically below by histogram of leakage particle size) were found in the H-ICT group except for a few in the L-ICT group, and reduced perfusion to vessel-like structural units (36–200 μm or 400–600 μm) was rarely found in the H-ICT group but occasionally found in the L-ICT group (Figs. 7B, C).

At week 2 post-induction, the angiograms in the CON group demonstrated dilated vessel-like structural units (>600 μm) surrounded by both numerous small size vessel-like structural units (36–200 μm) and numerous medium-sized widespread leakage-particle-like structural units (200–400 μm), when compared to those at baseline (Fig. 7D). The increased small size vessel-like structural units (36–200 μm) could be explained by angiogenesis under local hypoxia. Relative to those in the CON group at week 2 post-induction, dilated vessel-like structural units surrounded by many small size vessel-like structural units (36–200 μm) and numerous medium-sized widespread leakage-particle-like structural units (200–400 μm) were not found in the H-ICT group but moderate in the L-ICT group, and reduced perfusions to vessel-like structural units (400–600 μm) were rarely found in the H-ICT group but occasionally found in the L-ICT group (Figs. 7E, F).

Examination of size distribution of extravascular leakage particles

Extravascular leakage particles during perfusion for micro-CT-based angiography were more common in the CON group after induction, whereas these were rarely found in the H-ICT group and very occasionally found in the L-ICT group after induction (Figs. 6D, E). All histograms showed the size of the leakage particles ranged between 200 μm and 400 μm (Figs. 7G, H).

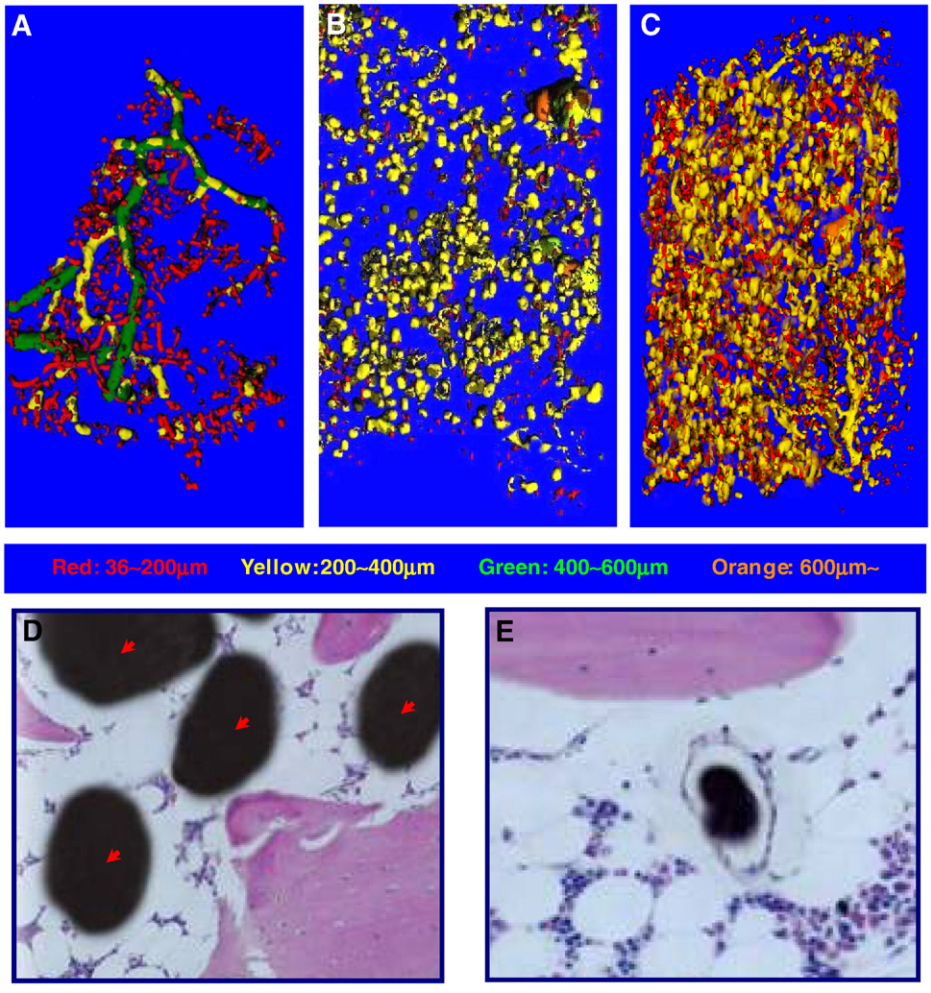

Fig. 6. Representative 3-D angiograms from micro-CT-based angiography and examination of perfused leakage particles for micro-CT-based angiography. (A) Vascular pattern at baseline and the H-ICT group at week 2 post-induction. (B) Vascular pattern in the CON group at week 1 post-induction. (C) Vascular pattern in the CON group at week 2 post-induction. Representative histology images of particles (indicated by arrow) were extravascularly distributed in the CON group at week 2 post-induction (D), whereas particles were intravascularly distributed in the H-ICT group at week 2 post-induction (E). Leakage particles mainly ranged from 200 to 400 μm. Note: * $p<0.05$. ● CON group, ♦ L-ICT group, and ■ H-ICT group. Black curve is representative of the H-ICT group and gray curve is representative of the CON group.

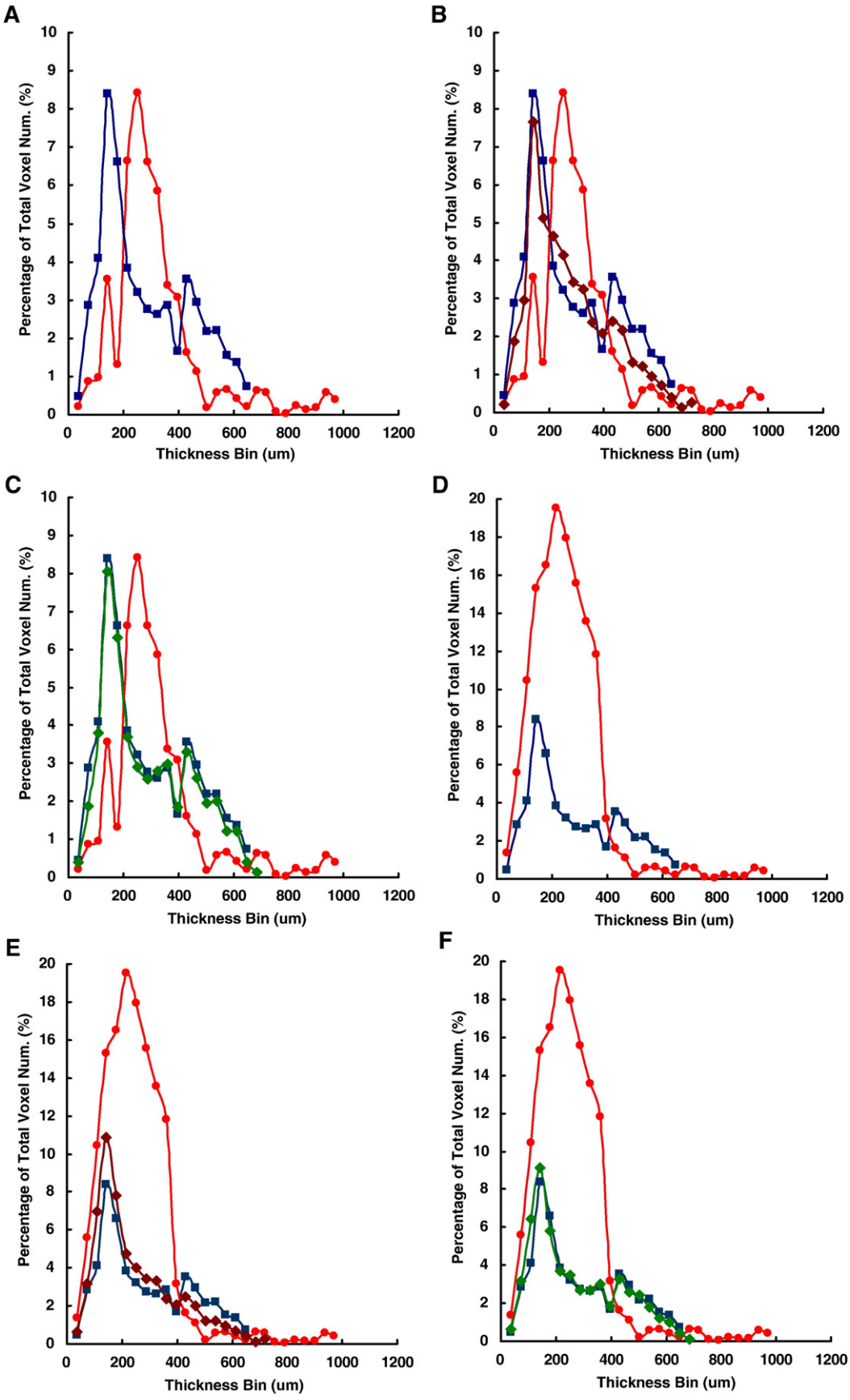
A
B
C
D
E
F
Percentage of Total Voxel Num. (%)
Thickness Bin (um)
0
200
400
600
800
1000
1200

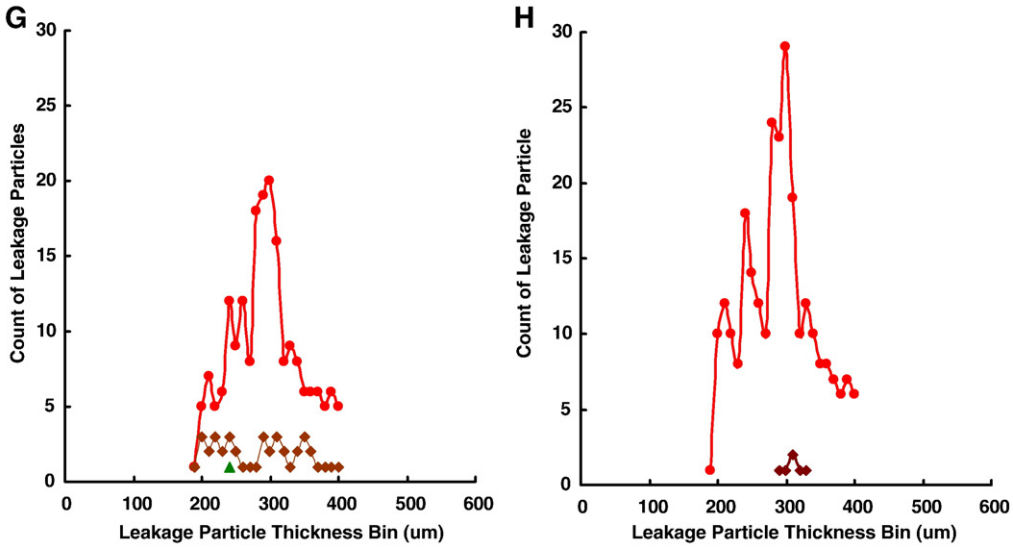

Fig. 7. Representative histograms of angiographic structural units from micro-CT-based angiography and representative histograms of extravascular leakage particles during perfusion for micro-CT-based angiography. (A) In the CON group, angiographic structural units ranging from 400 to 600 μm or 36–200 μm were less prevalent at week 1 post-induction than at baseline, whereas angiographic structural units ranging from 200 to 400 μm were more at week 1 post-induction than at baseline. (B) Angiographic structural units ranging from 36 to 200 μm or 400–600 μm were slightly less in the L-ICT group at week 1 post-induction than at the baseline. (C) No difference in the pattern of angiographic structural units between the baseline before induction and the H-ICT group at week 1 post-induction. (D) Angiographic structural units ranging from 400 to 600 μm were less prevalent in the CON group at week 2 post-induction than at the baseline, whereas angiographic structural units ranging from 36 to 200 μm were more prevalent in the CON group at week 2 post-induction than at the baseline. (E) Angiographic structural units ranging from 400 to 600 μm were slightly lower in the L-ICT group at week 2 post-induction than that at baseline, whereas angiographic structural units ranging from 36 to 200 μm were slightly prevalent than at the baseline. (F) No difference in the pattern of angiographic structural units between the baseline and the H-ICT group at week 2 post-induction. Representative histograms of extravascular leakage particles mainly ranged from 200 to 400 μm. Extravascular leakage particles were found more in the CON group compared to those in either the H-ICT or L-ICT group at week 1 (G) and week 2 post-induction (H). Note: Red circle indicates the CON group at week 1 post-induction, blue square indicates baseline before induction, brown rhombus indicates the L-ICT group, and green rhombus indicates the H-ICT group.

Local VEGF-A expression

Weak (+) or absent (−) immunoreactivity was found at baseline before induction. In the CON group, moderate (++) immunoreactivity located in both marrow cells and endothelium (confirmed by CD31) was found at week 1 post-induction, with strong immunoreactivity (+++) being found until week 2 post-induction. In the L-ICT group, immunoreactivity was found weak (+) or moderate (++) at week 1 post-induction, and weak (+) at week 2 post-induction. In the H-ICT group, immunoreactivity was weak (+) at week 1 post-induction, and weak (+) or absent (−) at week 2 post-induction. Representative changes in graded estimation for local VEGF-A expression in each group for bone marrow (Figs. 2E, F) and endothelium is shown (Figs. 2G, H).

Discussion

This was the first experimental study that demonstrated dose-dependent effect of a novel semisynthesized small molecule Icaritin on reducing incidence of steroid-associated ON in rabbits with inhibition of both intravascular thrombosis and extravascular lipid-deposition for maintaining integrity of intraosseous vasculature.

Dose-dependent effect of Icaritin on reducing steroid-associated ON risk with safety

The results of the calculated ON incidence indicates that the semisynthesized Icaritin is potentially an effective agent for reducing risk of steroid-associated ON in dose-dependent manner at the employed dosages (5 mg/kg and 10 mg/kg) (Figs. 2A and 3A). This is comparable to the prevention effect of Epimedium-derived flavonoids at employed dosages (10 mg/kg and 20–40 mg/kg) shown in our previous studies [13,14]. This study also provides experimental explanation for the previously noted clinical observation that ON prevalence was lower in SARS patients frequently prescribed crude extract of Epimedium in southern China than those seldom prescribed crude extract of Epimedium in northern China [10,11,18]. On the other hand, no significant difference in the ON extent among the three groups (Fig. 3B) was observed suggesting that a threshold exists beyond which ON is initiated, which is consistent with the findings in our recent study [13] and other researchers' study [9]. It also indicated that Icaritin was able to modulate the ON threshold. However, once the threshold was reached, Icaritin had little effect on occurrence of ON.

Recently, toxicity, in the form of organ bleeding, is a major concern following administration of a combination of an anticoagulant and a lipid-lowering agent for prevention of steroid-induced osteonecrosis development even though the efficacy of such a pharmaceutical combination strategy was experimentally confirmed [9]. In this study, Icaritin was safe throughout the observation period, with no evidence by any hepatocyte injury, bleeding or accidental death when using the two different Icaritin dosages.

Dose-dependent effect of Icaritin on inhibition of intravascular thrombosis

Icaritin was able to dose-dependently inhibit intravascular thrombosis (Fig. 3C), as evidenced by the increased thrombotic vessel count in the CON group which was attenuated in the L-ICT group and prevented in the H-ICT group (Figs. 2B, C).

Endothelium injury is recognized to be an important initial contributor to intravascular thrombosis. Soluble TM in plasma is an index of endothelial injury. Endothelium TM is a cell surface glycoprotein that is primarily expressed in endothelial cells and, along with protein C, plays a role in counteracting both hypercoagulation and hypofibrinolysis after endothelial cell injury, which maintain balance between coagulation and fibrinolysis [19]. In the present

study, a significant increase in TM in the CON group at week 1 post-induction was found (Fig. 4A), consistent with other study [20]. Our results also indicated that Icaritin was able to prevent endothelium from injury in a dose-dependent manner, as seen by the significantly increased TM in the CON group being attenuated in the L-ICT group and almost prevented in the H-ICT group at week 1 post-induction.

Oxidative stress has been identified as an important mechanism contributing to endothelium injury during steroid-associated ON occurrence [6,21]. GSH/LPO in plasma is a biochemical marker indicating level of oxidation stress [22]. GSH stabilizes lysosomal membrane suppressing vascular endothelium injury by inhibiting increase in lipoperoxides and maintaining cellular oxidation balance in favor of reduction [23–25]. LPO is generated by hyperoxidation of lipids, a biochemical indicator of tissue injury by active oxygens, closely associated with vascular injury [26,27]. In the present study, a significant decrease in GSH/LPO in CON group at week 1 post-induction was found (Fig. 4D), which was consistent with the findings of an experimental study of steroid-induced ON in rabbits [6]. The close correlation between GSH/LPO and TM ($R^2=0.78$) at 1 week post-induction strongly suggested that activated oxidative stress was involved in endothelium injury at an early stage during steroid-associated ON development. Our results also indicated that Icaritin was able to protect the endothelium from oxidative stress in a dose-dependent manner, as shown by a significant decrease in GSH/LPO in the CON group which was attenuated in the L-ICT group and almost negated in the H-ICT group at week 1 post-induction. This implied a protective effect of Icaritin on intravascular endothelium injury resulting from activated oxidative stress. This is not unexpected given that several flavonoids family agents derived from herbs have been identified as potential therapeutic antioxidants in different animal models [28–30].

Regarding coagulation and fibrinolysis secondary to endothelium injury, APTT is an index of coagulation, and tPA/PAI-I is an index of fibrinolysis. Imbalance between coagulation and fibrinolysis may predispose intravascular thrombosis. In the present study, a significant decrease in APTT level and tPA/PAI-I level in the CON group at week 1 post-induction was found (Fig. 4B), which was in accordance with clinical findings in steroid-associated ON patients [5]. This study also indicated that Icaritin was able to dose-dependently counteract both hypercoagulation and hypofibrinolysis at an early stage during steroid-associated ON development, as evidenced by the significantly decreased level of APTT and tPA/-I in the CON group being attenuated in the L-ICT group and almost prevented in the H-ICT group at week 1 post-induction.

Dose-dependent effect of Icaritin on inhibition of extravascular lipid-deposition

The specific histopathological examination suggested that Icaritin was able to inhibit extravascular lipid deposition in a dose-dependent manner (Fig. 3D), as evidenced by the significantly increased fat cell area fraction in the CON group being attenuated in the L-ICT group and prevented in the H-ICT group (Figs. 2C, D).

Regarding pathogenesis of extravascular lipid deposition during the early stage of steroid-associated ON development, the imbalance between local adipogenesis and lipid transportation from peripheral tissue is regarded as an important contributory event [4,7,31], as characterized by both elevated adipogenesis and lowered lipid transportation from peripheral tissue.

In this study, a high level of adipocyte positive colonies (an adipogenic potential index) and LDL/HDL (a lipid-transportation index) was used to reflect excessive adipogenesis and increased lipid transport to peripheral tissue, respectively [7]. It was shown that both excessive adipogenesis and lowered lipid transportation from peripheral tissue occurred at the early stage of steroid-associated ON development (Figs. 4E, F), as evidenced by the significantly increased level of adipocyte positive colonies and LDL/HDL in the CON group at week 1 post-induction. These findings were consistent with our previously published data [12,13] and with another recently reported study [31]. The results also indicated that Icaritin was able to counteract both elevated adipogenesis and lowered lipid transportation from peripheral tissue in a dose-dependent manner, as evidenced by the significant increase in adipocyte positive colonies and LDL/HDL in the CON group being attenuated in the L-ICT group and almost prevented in the H-ICT group at week 1 post-induction.

PPARgamma, as a transcription factor, has been proposed to play a central role in steroid-associated adipogenesis, which is support by both in vitro [8] and in vivo studies [32]. In the present study, a significant increase in PPARgamma protein expression in the CON group at week 1 post-induction was found (Figs. 4G, H), corresponding to an up-regulated PPARgamma expression at mRNA level during steroid-associated ON development in our published animal studies [13,14]. The close correlation between the up-regulated PPARgamma expression and increased adipocyte positive colonies ($R^2=0.86$) at week 1 post-induction in the present study strongly indicated that adipogenic protein PPARgamma was involved in the pathogenic mechanism of excessive extravascular adipogenesis at early stage of steroid-associated ON development. Our results also indicated that Icaritin was able to dose-dependently down-regulate PPARgamma protein expression, as evidenced by the significantly up-regulated PPARgamma protein expression in the CON group which was attenuated in the L-ICT group and almost prevented in the H-ICT group at week 1 post-induction, suggesting that suppression of PPARgamma protein expression contributes to the inhibitory effect of Icaritin on extravascular adipogenesis for lipid deposition. This is not surprising given that a series of herb-derived flavonoid/isoflavone family agents have been shown to be potential down-regulators of PPARgamma for anti-adipogenic [33].

Protective effect of Icaritin on intact intraosseous vascularity

Theoretically, vascularization insufficiency may not be sufficient to meet the oxygen and nutrient requirements of homeostatic tissue metabolism. Alternatively, excessive permeability, i.e. hyperpermeability, may induce high interstitial fluid pressure minimizing tissue perfusion and hindering local oxygen and nutrient delivery [34].

Dynamic contrast-enhanced MRI indicated insufficient vascular perfusion at an early stage, as evidenced by the significantly decreased PEP in the CON group at week 1 post-induction (Figs. 5A, B, D). Structurally, micro-CT based angiography suggested a prominent decrease in perfused vessels, as evidenced by few vessel-like structural units (36–200 μm or 400–600 μm) excluding leakage-particle-like structural units (200–400 μm) at week 1 post-induction compared to those at baseline (Figs. 6A,B, and 7A). The consistency in "vascular quantity" between dynamic contrast-enhanced MRI based functional evidence and micro-CT based structural evidence at an early stage indicated impairment of local arterial supply, which was reflected by the up-regulated VEGF expression in situ at week 1 post-induction (Figs. 2E–H). VEGF is an important signaling protein for physiological and pathological angiogenesis under hypoxia condition [35]. The results also indicated that Icaritin was able to dose-dependently maintain "vascular quantity" at an early stage, as evidenced by the following three functional-, structural-, and molecular-level evidences. First, the significantly decreased PEP in the CON group was attenuated in the L-ICT group and almost prevented in the H-ICT group at week 1 post-induction (Figs. 5A–C). Second, the reduced perfusion to vessel-like structural units (36–200 μm or 400–600 μm) was hardly observed in the H-ICT group but was occasionally in the L-ICT group at week 1 post-induction (Figs. 7B, 5C). Third, the moderate (++) immunoreactivity in the CON group was attenuated to (+/++) in the L-ICT group and prevented to (+) in the H-ICT group at week 1 post-induction, suggesting that local hypoxia was relieved by Icaritin (Figs. 2E–H).

At week 2 post-induction, considerable neovasculature was seen in the CON group, as evidenced by the significantly increased PEP over baseline (Figs. 5A–C) and the presence of numerous small size vessel-like structural units (36–200 μm) compared to baseline (Fig. 7D). This could be explained by local hypoxia-induced angiogenesis, as evidenced by local VEGF expression which was maintained at high level in the CON group throughout the experimental period. Icaritin was able to continuously relieve local hypoxia condition during steroid-associated ON development, as reflected by the continuously maintained high expression of VEGF in the CON group being attenuated in the L-ICT group and prevented in the H-ICT group throughout the experimental period (Figs. 2E–H).

Effect of Icaritin on relieving intraosseous vasculature hyperpermeability

Dynamic contrast-enhanced MRI based permeability index suggested the presence of hyperpermeability in the CON group at an early stage, as evidenced by the significantly increased PSρ in the CON group at week 1 post-induction (Figs. 5A, B, D). Micro-CT based angio-graphy indicated the presence of many medium-sized disseminated leakage-particle-like structural units (200–400 μm) at week 1 post-induction compared to baseline (Fig. 7A). This consistency in "vascular permeability" between dynamic contrast-enhanced MRI based functional evidence and micro-CT based structural evidence suggested that local impairment of local blood supply in the CON group at an early stage could be secondary to endothelium injury, a likelihood that was supported by a significant increase in serum TM in the CON group at week 1 post-induction. These findings also concur with a recent work reporting an increase in vascular permeability in steroid-induced ON model [6]. Our results also indicated that Icaritin was able to control "vascular permeability" at an early stage in a dose-dependent manner, as supported by the following two functional- and structural-level evidences: 1) the significantly increased PSρ in the CON group was attenuated in the L-ICT group and almost prevented in the H-ICT group at week 1 post-induction (Figs. 5A, B, D); and 2) nu-merous medium-sized disseminated leakage-particle-like structural units (200–400 μm, and confirmed histologically as by leakage particles) (Figs. 7G, 7H) in the CON group were not found in the H-ICT group but found only occasionally in the L-ICT group at week 1 post-induction (Figs. 7B, C).

At week 2 post-induction, worsening hyperpermeability was apparent, as shown by the significantly increased PSρ and the presence of more small-sized vessel-like structural units (36–200 μm) compared to week 1 post-induction in the CON group (Figs. 5A, B, D). The worsening hyperpermeability could be explained by continuous high level of VEGF expression, which was attributed to VEGF-induced angiogenesis accompanied by a vascular permeability response [36–38], also reflecting unrelieved local hypoxia during steroid-associated ON development. Icaritin was able to continuously control "vascular permeability" in a dose-dependent manner at week 1 post-induction, as shown by a significant increase in PSρ from week 1 to week 2 post-induction in the CON group being prevented among the L-ICT and H-ICT group (Figs. 5A, B, D), and numerous medium-sized disseminated leakage-particle-like structural units (200–400 μm) (Figs. 7G, H) in the CON group were not shown in the H-ICT group but only occasionally in the L-ICT group at week 2 post-induction (Figs. 7E, F).

Conclusion

The semisynthesized small molecule Icaritin exerted a dose-dependent effect on inhibition of intravascular thromboses by counteracting hypercoagulation–hypofibrinolysis and extravascular lipid-deposition by counteracting excessive adipogenesis and prominent lipid transport to peripheral tissue, thereby helping to maintain intraosseous vascular integrity, and reduce incidence of steroid-associated ON. Icaritin seemed to act by suppression of up-regulated proliferator-activated receptor-gamma expression to counteract extravascular adipogenesis and protection of endothelium from injury of activated oxidative stress.

Conflict of interest

None of the authors have any conflict of interest.

Acknowledgments

We thank Dr. HY Yeung for providing Micro-CT support. We also thank Dr. CW Chan for providing expertise in histology, and Dr. H Qiu for advice on statistical analysis. We are grateful to all members of the Clinical Immunology Unit in the Chinese University of Hong Kong and Dr. SL Peng in the Department of Orthopedics & Traumatology in Hong Kong University for providing technical support for immunoblotting.

This study was supported by the "Hong Kong Research Grant Council (CUHK4503/06M)", the "Hong Kong Innovation and Technology Support Programme (ITS/012/06)", the Earmarked Research Grant (Project Ref. No. 472508), and the Earmarked Research Grant (Project Ref. No. 478508). This study was also supported by NSFC-RGC Grant (Project Reference No. : N_CUHK405/08).

References

[1] Aaron RK. Osteonecrosis: etiology, pathophysiology and diagnosis. In: Callaghan JJ, Rosenberg AG, Rubash HE, editors. The adult hip. Philadelphia: Lippincott-Raven; 1998. p. 457.
[2] Assouline-Dayan Y, Chang C, Greenspan A, Shoenfeld Y, Gershwin ME. Pathogenesis and natural history of osteonecrosis. Semin Arthritis Rheum 2002;32:94–124.
[3] Lieberman JR, Berry DJ, Mont MA, et al. Osteonecrosis of the hip: management in the 21st century. Instr Course Lect 2002;52:337–55.
[4] Wang GJ, Cui Q, Balian G. The pathogenesis and prevention of steroid-induced osteonecrosis. Clin Orthop Relat Res 2000;370:295–310.
[5] Glueck CJ, Freiberg RA, Fontaine RN. Hypofibrinolysis, thrombophilia, osteonecrosis. Clin Orthop Relat Res 2001;386:19–33.
[6] Ichiseki T, Matsumoto T, Nishino M, Kaneuji A, Katsuda S. Oxidative stress and vascular permeability in steroid-induced osteonecrosis model. J Orthop Sci 2004;9:509–15.
[7] Miyanishi K, Yamamoto T, Irisa T. A high low-density lipoprotein cholesterol to high-density lipoprotein cholesterol ratio as a potential risk factor for corticosteroid-induced osteonecrosis in rabbits. Rheumatology (Oxford) 2001;40:196–201.
[8] Li X, Jin L, Cui Q. Steroid effects on osteogenesis through mesenchymal cell gene expression. Osteoporos Int 2005;16:101–8.
[9] Motomura G, Yamamoto T, Miyanishi K, Jingushi S, Iwamoto Y. Combined effects of an anticoagulant and a lipid-lowering agent on the prevention of steroid-induced osteonecrosis in rabbits. Arthritis Rheum 2004;50:3387–91.
[10] Griffith JF, Antonio GE, Kumta SM. Osteonecrosis of hip and knee in patients with severe acute respiratory syndrome treated with steroids. Radiology 2005;235:168–75.
[11] Li ZR, Sun W, Qu H. Clinical research of correlation between osteonecrosis and steroid. Zhonghua Wai Ke Za Zhi 2005;43:1048–53.
[12] Qin L, Zhang G, Sheng H. Multiple imaging modalities in evaluation of experimental osteonecrosis induced by a combination of lippolysaccharide and methylprednisolone. Bone 2006;39:863–71.
[13] Zhang G, Qin L, Sheng H, Yeung KW, James G, Leung KS. Epimedium-derived phytoestrogen exert beneficial effect on preventing steroid-associated osteonecrosis in rabbits with inhibition of both thrombosis and lipid-deposition. Bone 2007;40:685–92.
[14] Qin L, Zhang G, Sheng H, et al. Phytoestrogenic compounds for prevention of steroid-associated osteonecrosis. J Musculoskelet Neuronal Interact 2008; 8 (In Print)
[15] Setchell KD, Brown NM, Desai P, et al. Bioavailability of pure isoflavones in healthy humans and analysis of commercial soy isoflavone supplements. J Nutr 2001;131 (Suppl 4):1362S–75S.
[16] Yuan JP, Wang JH, Liu X. Metabolism of dietary soy isoflavones to equol by human intestinal microflora—implications for health. Mol Nutr Food Res 2007;51:765–81.
[17] Park JS, Park HY, Rho HS, Ahn S, Kim DH, Chang IS. Statistically designed enzymatic hydrolysis for optimized production of icariside II as a novel melanogenesis inhibitor. J Microbiol Biotechnol 2008;18:110–7.
[18] http://www.tcm120.com/tcm/sars/zzyfz/zzyfz0702_1.htm.
[19] Ejiri S, Eguchi Y, Kishida A. Cellular distribution of thrombomodulin as an early marker for warm ischemic liver injury in porcine liver transplantation: Protective effect of prostaglandin I2 analogue and tauroursodeoxycholic acid. Transplantation 2001; 27: 71:721–726.
[20] Kabata T, Matsumoto T, Nishio M. Histopathological and immunohistochemical study of femoral bone and bone marrow tissues in steroid treated rabbits. J Neurol Orthop Med Surg 2000;20:41–6.
[21] Ichiseki T, Ueda Y, Katsuda S, Kitamura K, Kaneuji A, Matsumoto T. Oxidative stress by glutathione depletion induces osteonecrosis in rats. Rheumatology (Oxford) 2006;45:287–90.

[22] Weinbroum AA, Kidron A, Hochhauser E, Hochman A, Rudick V, Vidne BA. Liver glutathione level influences myocardial reperfusion injury following liver ischemia-reperfusion. Med Sci Monit 2001;7:1137–44.
[23] Burk RF, Patel K, Lane JM. Reduced glutathione protection against rat liver microsomal injury by carbon tetrachloride: dependence on O2. Biochem J 1983; 215:441–5.
[24] Willis ED. Mechanisms of lipid peroxide formation in animal tissues. Biochem J 1996;99:667–76.
[25] Jones Jr JP. Intravascular coagulation and osteonecrosis. Clin Orthop 1992;277: 41–53.
[26] Sasaguri Y, Nakashima T, Morimatsu M, et al. Injury to cultured endothelial cells from human umbilical vein by linoleic acid hydroperoxide. J Appl Biochem 1984;6: 144–50.
[27] Uzel N, Sivas A, Uysal M. Erythrocyte lipid peroxidation and glutathione peroxidase activities in patients with diabetes mellitus. Horm Metab Res 1987; 19:89–90.
[28] Castillo C, Salazar V, Ariznavarreta C, Vara E, Tresguerres JA. Effect of isoflavone administration on age-related hepatocyte changes in old ovariectomized female Wistar rats. Phytomedicine 2006;13:468–76.
[29] Nencini C, Giorgi G, Micheli L. Protective effect of silymarin on oxidative stress in rat brain. Phytomedicine 2007;14:129–35.
[30] Singh JP, Selvendiran K, Banu SM, Padmavathi R, Sakthisekaran D. Protective role of apigenin on the status of lipid peroxidation and antioxidant defense against hepatocarcinogenesis in Wistar albino rats. Phytomedicine 2004;11: 309–14.
[31] Yin L, Li YB, Wang YS. Dexamethasone-induced adipogenesis in primary marrow stromal cell cultures: mechanism of steroid-induced osteonecrosis. Chin Med J (Engl) 2006;119:581–8.
[32] Cui Q, Wang GJ, Su CC, Balian G. The Otto Aufranc award. Lovastatin prevents steroid induced adipogenesis and osteonecrosis. Clin Orthop Relat Res 1997;344: 8–19.
[33] Hsu CL, Yen GC. Effects of flavonoids and phenolic acids on the inhibition of adipogenesis in 3T3-L1 adipocytes. J Agric Food Chem 2007;55:8404–10.
[34] Netti PA, Roberge S, Boucher Y, Baxter LT, Jain RK. Effect of transvascular fluid exchange on pressure-flow relationship in tumors: a proposed mechanism for tumor blood flow heterogeneity. Microvasc Res 1996;52:27–46.
[35] Asahara T, Takahashi T, Masuda H, et al. VEGF contributes to postnatal neovascularization by mobilizing bone marrow-derived endothelial progenitor cells. EMBO J 1999;18:3964–72.
[36] Marti HJ, Bernaudin M, Bellail A, et al. Hypoxia-induced vascular endothelial growth factor expression precedes neovascularization after cerebral ischemia. Am J Pathol 2000;156:965–76.
[37] van Bruggen N, Thibodeaux H, Palmer JT, et al. VEGF antagonism reduces edema formation and tissue damage after ischemia/reperfusion injury in the mouse brain. J Clin Invest 1999;104:1613–20.
[38] Weis SM, Cheresh DA. Pathophysiological consequences of VEGF-induced vascular permeability. Nature 2005;437:497–504.
[39] Benson RE, Catalfamo JL, Brooks M, Dodds WJ. A sensitive immunoassay for von Willebrand factor. J Immunoass 1991;12:371–90.
[40] Benson RE, Catalfamo JL, Dodds WJ. A multispecies enzyme-linked immunosorbent assay for von Willebrand's factor. J Lab Clin Med 1992;119:420–7.
[41] Sheng H, Zhang G, Cheung WH, et al. Elevated adipogenesis of marrow mesenchymal stem cells during early steroid-associated osteonecrosis development. J Orthop Surg 2007;2:15.
[42] Bogin L, Margalit R, Mispelter J, Degani H. Parametric imaging of tumor perfusion using flow- and permeability-limited tracers. J Magn Reson Imaging 2002;16: 289–99.
[43] Yamamoto T, Hirano K, Tsutsui H. Corticosteroid enhances the experimental induction of osteonecrosis in rabbits with Shwartzman reaction. Clin Orthop Relat Res 1995;316:235–43.
[44] Parfitt AM, Drezner MK, Glorieux FH, et al. Bone histomorphometry: standardization of nomenclature, symbols, and units. Report of the ASBMR Histomorphometry Nomenclature Committee. J Bone Miner Res 1987;2:595–610.
[45] Sternberger LA, Sternberger NH. The unlabeled antibody method: comparison of peroxidase-antiperoxidase with avidin-biotin complex by a new method of quantification. J Histochem Cytochem 1986;5:599–605.